A CONSTITUTIVE MODEL FOR THERMOPLASTICS WITH SOME APPLICATIONS

Arild Holm Clausen[1,2], Mario Polanco-Loria[1,3], Torodd Berstad[1,2,3] and Odd Sture Hopperstad[1,2]

[1] *Structural Impact Laboratory (SIMLab) , Norwegian University of Science and Technology (NTNU), NO-7491 Trondheim, Norway*
[2] *Department of Structural Engineering, NTNU, NO-7491 Trondheim, Norway*
[3] *SINTEF Materials and Chemistry, NO-7465 Trondheim, Norway*

ABSTRACT

A constitutive model for thermoplastics is outlined in this paper. The model consists of two parts: A hyperelastic-viscoplastic response due to intermolecular resistance denoted Part A, and an entropic hyperelastic response due to re-orientation of molecular chains called Part B. Both parts are developed within a framework for finite strains. The main constituents are the Neo-Hookean model describing large elastic deformations, the pressure-sensitive Raghava yield function, a non-associated visco-plastic flow potential and Anand's stress-stretch relation representing the intramolecular stiffness. The 11 non-zero coefficients of the model are identified from uniaxial tension and compression tests on two materials, HDPE and PVC, which are respectively semi-crystalline and amorphous thermoplastics. Subsequently, it is employed in numerical simulations of three-point bending tests on the same materials. The model gives satisfactory predictions when compared to experimental behaviour.

1. INTRODUCTION

This paper presents a hyperelastic-viscoplastic constitutive model for thermoplastics [1]. It is partly based on a model described by Boyce et al. [2], but with some modifications. The idea of separating the response into inter-molecular and intra-molecular contributions, originally proposed by Haward and Thackray [3], is adopted. In our model, the energy-elastic deformation is represented with a Neo-Hookean model. Further, Raghava's pressure-dependent yield function is introduced [4], and a non-associated flow rule is assumed, applying a Raghava-like plastic potential. The entropy-elastic deformation is modelled with Anand's stress-stretch relation [5]. The model involves 12 coefficients, whereof 11 are non-zero. They can be determined from uniaxial tests in tension and compression.

Section 2 of this paper provides a brief outline of the constitutive model. Thereafter, material tests on a high-density polyethylene (HDPE) and polyvinylchloride (PVC) are reviewed in Section 3. The results from these tests are used to calibrate the constitutive model, see Section 4. Thereafter, the model is employed in numerical simulations of a tension test specimen and a three-point bending test. The predictions are compared with experimental results in Section 5. Finally, Section 6 provides some conclusions and possible ideas for further work.

The model is implemented as a user-defined model in LS-DYNA [6], so far working for brick elements. A set of numerical verification tests has been carried out [1], showing that the model is able to capture pressure dependency, volumetric plastic strain, strain rate sensitivity, and induced strain anisotropy.

2. OUTLINE OF CONSTITUTIVE MODEL

Figure 1 summarises the main constituents of the constitutive model proposed by Polanco-Loria et al. [1]. The material response is assumed to have two resistances A and B, which represent the intermolecular and intramolecular (network) strength, respectively. Parts A and B are kinematically described by the same deformation gradient $\mathbf{F}$. The Cauchy stress tensor $\boldsymbol{\sigma}$ is obtained by summing the contributions of Parts A and B, i.e. $\boldsymbol{\sigma} = \boldsymbol{\sigma}_A + \boldsymbol{\sigma}_B$.

The deformation gradient $\mathbf{F}_A$ is decomposed into elastic and plastic parts, i.e. $\mathbf{F}_A = \mathbf{F}_A^e \cdot \mathbf{F}_A^p$. Similarly, the Jacobian J_A of Part A, representing the volume change, is decomposed as $J_A = \det \mathbf{F}_A = J_A^e J_A^p = J$. This decomposition of $\mathbf{F}_A$ means that the viscoplastic part of the model is formulated on an intermediate configuration $\bar{\Omega}_A$ defined by $\mathbf{F}_A^p$ [1]. A compressible Neo-Hookean material is chosen for the elastic part of the deformation, and the Cauchy stress tensor $\boldsymbol{\sigma}_A$ reads

$$\boldsymbol{\sigma}_A = \frac{1}{J_A^e}\left(\lambda_0 \ln J_A^e \, \mathbf{I} + \mu_0 [\mathbf{B}_A^e - \mathbf{I}]\right) \qquad (1)$$

where λ_0 and μ_0 are the classical Lamé constants of the linearized theory, $\mathbf{B}_A^e = \mathbf{F}_A^e \cdot (\mathbf{F}_A^e)^T$ is the elastic left Cauchy-Green deformation tensor, and $\mathbf{I}$ is the second order unit tensor. The coefficients λ_0 and μ_0 may alternatively be expressed as functions of Young's modulus E_0 and Poisson's ratio ν_0.

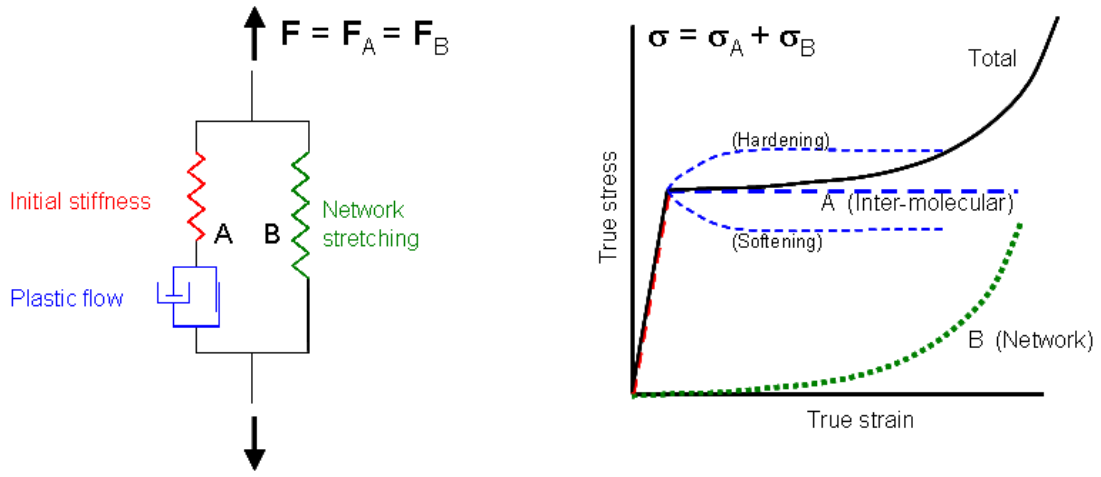

Figure 1: Constitutive model with inter-molecular (A) and network (B) contributions.

The yield criterion is assumed in the form

$$f_A = \bar{\sigma}_A - \sigma_T - R\left(\varepsilon_A^p\right) = 0 \tag{2}$$

where σ_T is the yield stress in uniaxial tension and $R\left(\varepsilon_A^p\right)$ is a term allowing for hardening or softening. It should be noted that the term $R\left(\varepsilon_A^p\right)$ was not included in the description of the model presented by Polanco-Loria et al. [1]. The equivalent stress $\bar{\sigma}_A$ accounts for the pressure-sensitive behaviour, commonly observed in polymeric materials, and it is defined according to Raghava et al. [4], viz.

$$\bar{\sigma}_A = \frac{(\alpha-1) I_{1A} + \sqrt{(\alpha-1)^2 I_{1A}^2 + 12\alpha J_{2A}}}{2\alpha} \tag{3}$$

The material parameter $\alpha = \sigma_C / \sigma_T \geq 1$ describes the pressure sensitivity, where σ_C is the uniaxial compressive yield strength of the material, and I_{1A} and J_{2A} are stress invariants related to respectively the total and the deviatoric Mandel stress tensor $\bar{\boldsymbol{\Sigma}}_A$ operating on the intermediate configuration $\bar{\Omega}_A$. More details, including relations between the different stress measures, are provided by Polanco-Loria et al. [1]. It is noted that the equivalent stress $\bar{\sigma}_A$ is equal to the von Mises – equivalent stress $\bar{\sigma} = \sqrt{3J_2}$ when $\alpha = 1$, i.e. $\sigma_C = \sigma_T$.

The term $R\left(\varepsilon_A^p\right)$ in Equation (2) reads

$$R\left(\varepsilon_A^p\right) = \left(\sigma_s - \sigma_T\right)\left[1 - \exp\left(-H\varepsilon_A^p\right)\right] \tag{4}$$

where σ_s is the saturated stress level of Part A, and the decay coefficient H is used to provide an optimum fit of the stress-strain curve between σ_T and σ_s. Clearly, Equation (4) represents hardening when $R\left(\varepsilon_A^p\right)$ is positive, while softening is obtained by selecting $\sigma_s < \sigma_T$.

It turned out that an associated flow rule predicts unrealistic large volumetric plastic strains. In order to control the plastic dilatation, a non-associated flow rule is introduced, applying a Raghava-like plastic potential function

$$g_A = \frac{(\beta-1) I_{1A} + \sqrt{(\beta-1)^2 I_{1A}^2 + 12\beta J_{2A}}}{2\beta} \geq 0 \tag{5}$$

where the material parameter $\beta \geq 1$ controls the volumetric plastic strain. Isochoric plastic behaviour is obtained in the special case of $\beta = 1$. A drawback of this choice of potential function is that it will predict plastic dilatation in compression as well as tension. Experimental observations on some materials indicate contraction in compression [7].

Finally, the plastic rate-of-deformation tensor is calculated from $\bar{\mathbf{D}}_A^p = \dot{\bar{\varepsilon}}_A^p \, \partial g_A / \partial \bar{\mathbf{\Sigma}}_A$. The equivalent plastic strain rate $\dot{\bar{\varepsilon}}_A^p$ is chosen as

$$\dot{\bar{\varepsilon}}_A^p = \begin{cases} 0 & \text{if} \quad f_A \le 0 \\ \dot{\varepsilon}_{0A} \left\{ \exp\left[\frac{1}{C} \left(\frac{\bar{\sigma}_A}{\sigma_T + R} - 1 \right) \right] - 1 \right\} & \text{if} \quad f_A > 0 \end{cases} \tag{6}$$

where R is the hardening term defined in Equation (4). The two coefficients C and $\dot{\varepsilon}_{0A}$ are easy to identify from uniaxial strain-rate tests.

The deformation gradient $\mathbf{F}_B$ of Part B, see Figure 1, represents the network orientation and it is assumed that the network resistance is hyperelastic. Following Anand [5], the Cauchy stress-stretch relation is given as

$$\boldsymbol{\sigma}_B = \frac{1}{J} \left[\frac{C_R}{3} \frac{\bar{\lambda}_L}{\bar{\lambda}} L^{-1} \left(\frac{\bar{\lambda}}{\bar{\lambda}_L} \right) \left(\mathbf{B}_B^* - \bar{\lambda}^2 \mathbf{I} \right) + \kappa \left(\ln J \right) \mathbf{I} \right] \tag{7}$$

where the Jacobian $J = J_B = \det \mathbf{F}$, and L^{-1} is the inverse function of the Langevin function defined as $L(\beta) = \coth \beta - 1/\beta$. The effective distortional stretch is $\bar{\lambda} = \sqrt{\mathrm{tr}\left(\mathbf{B}_B^*\right)/3}$, where $\mathbf{B}_B^* = \mathbf{F}_B^* \cdot (\mathbf{F}_B^*)^{\mathrm{T}}$ is the distortional left Cauchy-Green deformation tensor, and $\mathbf{F}_B^* = J_B^{-1/3} \mathbf{F}_B$ denotes the distortional part of $\mathbf{F}_B$. There are three constitutive parameters describing the intra-molecular resistance: C_R is the initial elastic modulus of Part B; $\bar{\lambda}_L$ is the locking stretch; and κ is a bulk modulus. The coefficient κ is fixed to the value 0 in the work presented herein, thereby ensuring that the stress state of Part B is deviatoric. By omitting Part A, however, the remaining Part B with $\kappa \neq 0$ may be applied for rubber modelling.

3. MATERIAL TESTS

Two thermoplastics were acquired as large extruded plates 2000mm × 1000mm × 10mm for application in this study: A semi-crystalline high-density polyethylene (HDPE), and an amorphous polyvinylchloride (PVC). The material test coupons in uniaxial tension and compression, see Figure 2, as well as specimens for the validation tests were machined from these plates. Material tests on these materials have already been reported by Moura et al. [7]. New tests were now performed, however, to incorporate any possible effects of storage time, and with a different design of test samples. Unlike the previous study [7], there was not machined any imperfection in the gauge part of the tension sample, and cylinder-shaped coupons were applied instead of cubes in the compression tests. More details are provided by Hovden [8] and Haugen [9].

The tests were carried out in a servo-hydraulic testing machine under displacement control. The applied velocity and hence the nominal strain-rate $\dot{e}$ were constant in each test, and the applied rates were 10^{-3}, 10^{-2} and 10^{-1} s^{-1} in both loading modes. In general, two parallel tests were performed in each case, and the scatter between these replicates was small.

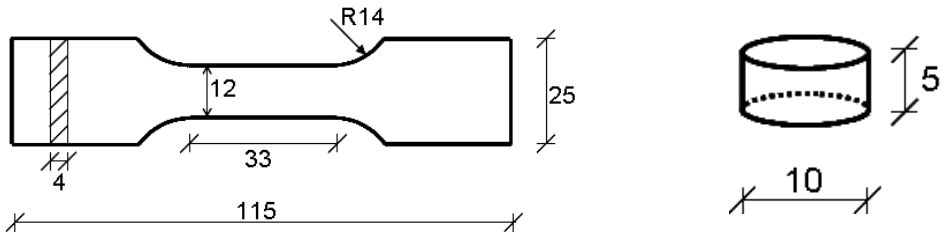

(a) (b)

Figure 2: (a) Tension test sample. (b) Compression test sample.

The acquisition system of the machine provided measurements of the cross-head displacement and force. The capacity of the load cell was 20 kN. Moreover, each test was monitored with a camera taking digital photos for a subsequent determination of the full-field in-plane deformations applying digital image correlation (DIC). This system facilitates the determination of true longitudinal and transverse strains, respectively ε_1 and ε_2, at the surface of the coupon facing the camera. Moura et al. [7] provide a more thorough description of the processing of the photos.

As shown by Hovden [8], Haugen [9] and also by Moura et al. [7], the transverse deformation of both materials is close to isotropic, i.e. $\varepsilon_2 = \varepsilon_3$. The true stress in the tension samples can therefore be calculated from

$$\sigma = \frac{F}{A} = \frac{F}{w_0 \exp(\varepsilon_2) \cdot t_0 \exp(\varepsilon_3)} = \frac{F}{A_0 \cdot \exp(2\varepsilon_2)} \tag{8}$$

where F is the force measured during the test, and $A_0 = w_0 t_0$ is the initial cross-section area of the sample. A digital sliding calliper provided the measures of w_0 and t_0 for each specimen, which was susceptible to differ slightly from the nominal dimensions shown in Figure 2(a). The true stress was calculated in the section experiencing the initial localization.

The DIC software was not applied in the compression tests. Similar to the tension specimens, the initial height h_0 and diameter d_0 were measured prior to each test. Assuming homogeneous deformation over the length of the sample, the longitudinal strain was found from the relation $\varepsilon_1 = \ln(h/h_0) = \ln(1-\Delta h/h_0)$, where Δh is the shortening as measured by the servo-hydraulic machine. The digital pictures were employed in the determination of the transverse deformation, as they provided a measure of the diameter increase Δd during the test. The transverse strain ε_2 is thus $\varepsilon_2 = \ln(d/d_0) = \ln(1+\Delta d/d_0)$. The current diameter d turned out to be the same over the height of the sample until $\varepsilon_1 \approx 0.5$, implying that rather large deformations were possible before any barrelling effect was present [8]. The last

equality of Equation (8) was used for calculation of the true stress in the compression tests as well, setting $A_0 = (\pi / 4) d_0^2$.

Representative stress-strain curves obtained at different nominal strain-rates in tension are shown in Figure 3, while compression data are presented in Figure 4. A significant strain-rate effect is present for both materials and loading modes. PVC experiences also a softening effect after yielding. Both materials are to some degree pressure dependent. PVC has higher yield strength in compression than in tension. The situation for HDPE is slightly more complicated. Without any local maximum point neither for the nominal nor the true stress-strain curves, the yield stress is conveniently determined from the classical Considère construction. It turns out that the yield stress is almost identical in tension and compression for HDPE. On the other hand, the evolution of hardening between true strains of 0.1 and 0.5 differs. Although not shown here, the full-field strain measurements also revealed that the deformation of HDPE is rather isochoric (volume preserving), while PVC dilates (volume increases) in tension [8].

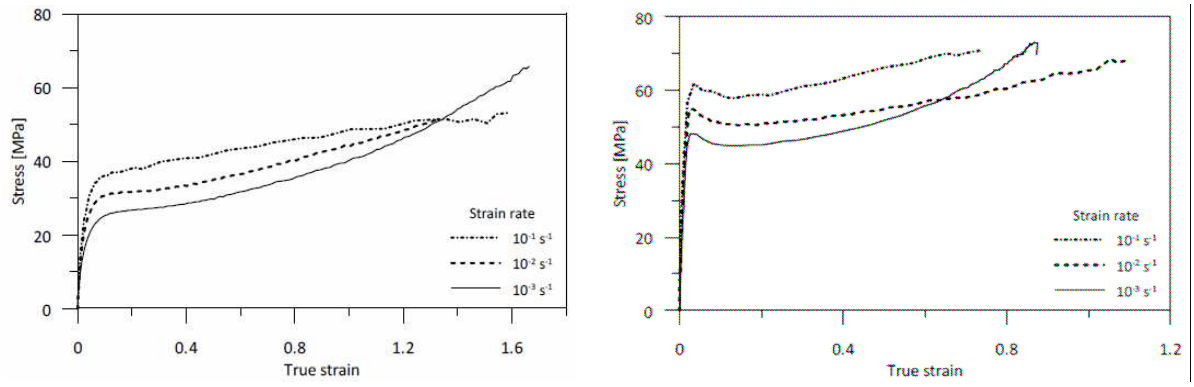

Figure 3: True stress-strain curves in tension [8]. (a) HDPE. (b) PVC.

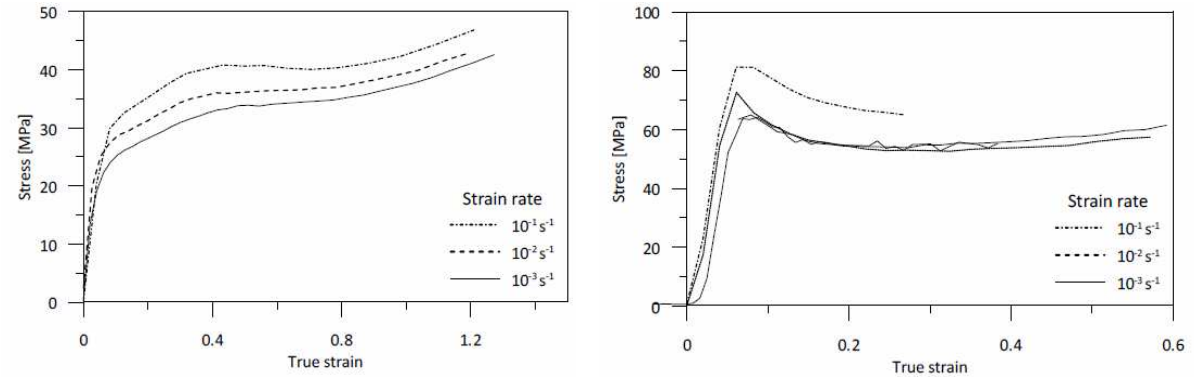

Figure 4: True stress-strain curves in compression [8]. (a) HDPE. (b) PVC.

4. CALIBRATION OF CONSTITUTIVE MODEL

The constitutive model depicted in Figure 1 involves 11 non-zero coefficients:

- Spring A: Two elastic coefficients E_0 (Young's modulus) and ν_0 (Poisson's ratio).
- Friction element A: The yield criterion applies the yield stress in tension σ_T, the ratio $\alpha = \sigma_C / \sigma_T$, and the hardening/softening parameters σ_s and H. Moreover, the coefficient β is employed to control the plastic dilatation.
- Dashpot A: Two strain-rate sensitivity parameters *C* and $\dot{\varepsilon}_{0A}$.
- Spring B: Two coefficients C_R (initial elastic modulus) and $\overline{\lambda}_L$ (locking stretch). The bulk modulus κ is fixed to the value 0, ensuring that the hydrostatic stress of Part B vanishes.

Details on the calibration procedure are provided by Hovden [8], and only a brief survey is given here. The measurements of transverse and longitudinal strains in tension give the parameters ν_0 and β. Further, one of the tension tests at the lowest strain-rate (10^{-3} s^{-1}) serves as the baseline case, wherefrom most of the remaining coefficients are identified. The local strain rate at yielding is taken as $\dot{\varepsilon}_{0A}$. The shape of the true stress-strain curve determines whether the hardening (HDPE) or softening (PVC) option of Equation (4) is to be adopted. Next, a plot of yield stresses in tension as function of the logarithm of strain-rate determines *C*. To obtain an optimum curve fit, the physical yield stress is assigned to σ_T for PVC, and to σ_s for HDPE, and the values of these coefficients are found from the plot by extrapolation of the linear regression curve to zero strain-rate. Thereafter E_0 and H are determined together with the remaining coefficients σ_T and σ_s. The Part B parameters C_R and $\overline{\lambda}_L$ require some calculation efforts. Part A as defined by the coefficients identified so far is subtracted from the baseline stress-strain curve, yet also recognizing that Part B does not represent any uniaxial rather a deviatoric stress state. Finally, α is the ratio between the yield stress in compression and tension. All parameters are gathered in Table 1.

Table 1: Coefficients for HDPE and PVC [8].

	E_0 (MPa)	ν_0	σ_T (MPa)	σ_s (MPa)	H	α	β	$\dot{\varepsilon}_{0A}$ (s^{-1})	C	C_R (MPa)	$\overline{\lambda}_L$
HDPE	800	0.40	13.0	23.9	39.6	1.00	1.04	0.0007	0.108	1.74	7.75
PVC	3000	0.30	46.8	37.8	15.0	1.30	1.27	0.001	0.070	5.50	1.92

5. VALIDATION OF CONSTITUTIVE MODEL

As a first step in the validation process, the tension test sample was modelled in LS-DYNA, applying 1084 eight-node brick elements [8] and the coefficients of Table 1. Considering the baseline test at strain rate 10^{-3} s^{-1}, Figure 5 shows comparisons between the force-displacement curves found from the tests and with LS-DYNA. Applying the digital pictures, the displacement was determined by considering how the distance between two defined points evolved during the test. Thus, these points served as an optical extensometer. The same points were selected in the numerical simulations. The agreement in Figure 5 is excellent, and, although not shown here, the model predicts also the necking of the sample in an adequate way.

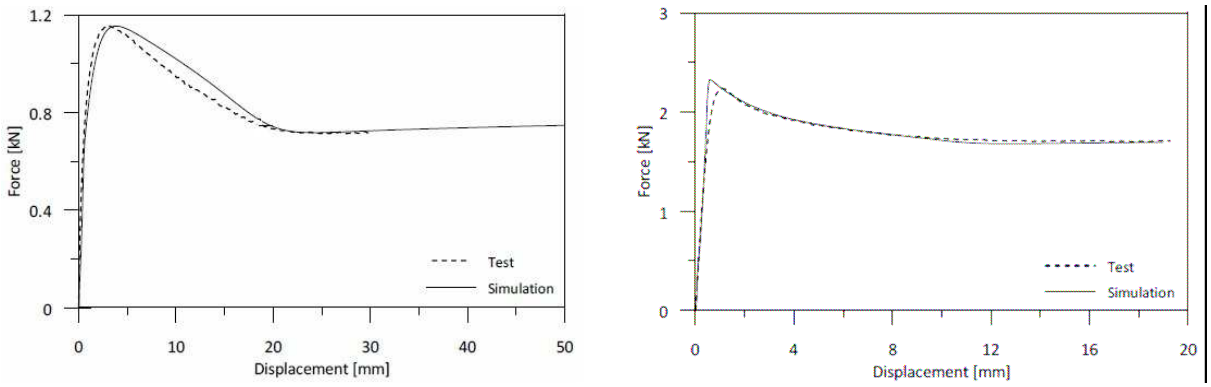

(a) (b)

Figure 5: Force-displacement curves in tension at 10^{-3} s^{-1}. Comparison of laboratory tests and numerical simulations [8]. (a) HDPE. (b) PVC.

Formally, a validation should apply other tests than those involved in the calibration, yet it is important for the subsequent numerical modelling that the validation tests are well-defined. Three-point bending tests are suitable for this purpose. The experimental set-up is shown in Figure 6. The rollers ensure that no bending moments are transferred to the supports. Four different plate thicknesses t = {4mm, 6mm, 8mm, 10mm} and two punch nose radii R = {3mm, 6mm} were applied. The bending tests were carried out in the same machine as was used in the material tests, and the cross-head velocity was 0.1 mm/s in all tests. Some of the tests with plate thickness 8mm and 10mm were painted with a speckled pattern and instrumented with a digital camera, facilitating determination of the strain field at the surface by means of DIC.

Utilising the two symmetry planes, ¼ of the plate was modelled with brick elements in LS-DYNA, applying 9 elements over the thickness and 25 elements in each of the in-plane directions. The coefficient of friction between the plate and steel parts was set to 0.1. Increasing the coefficient to 0.2 or lowering it to 0.01 did not give any significant difference in the results.

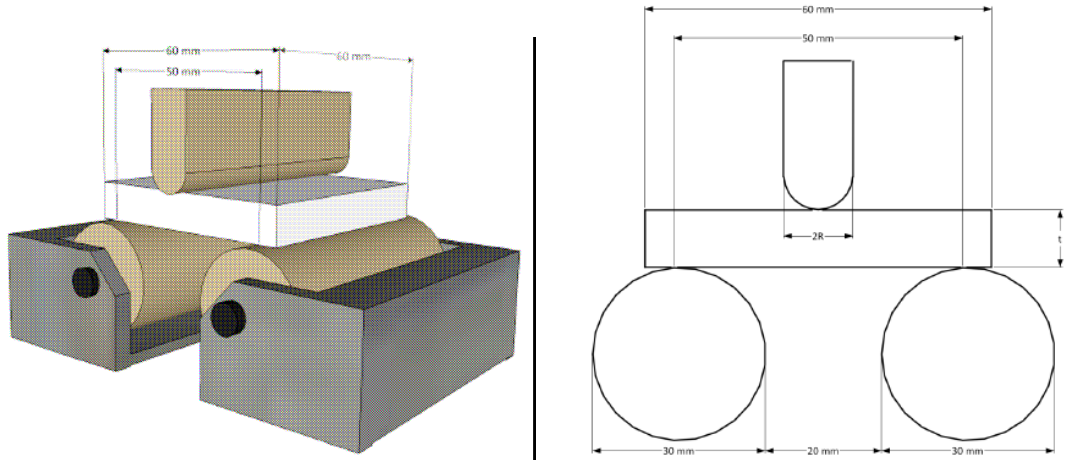

(a) (b)

Figure 6: Set-up for three-point bending tests [8]. (a) 3D sketch. (b) Drawing with dimensions.

Figure 7 shows a comparison between the force-displacement curves found in the experiments and the numerical simulations for a nose radius of R = 3mm. The thinnest plates, having thickness 4mm and 6mm, are addressed in this figure. The agreement is satisfactory, although some discrepancy is present at large deformations. The constitutive model assumes that the stress-strain curves have the same shape in both loading modes and at all strain-rates. It appears from Figures 3 and 4 that this is not the case. In particular, the hardening effect at compression strains between 0.1 and 0.5 is not captured by the model. Another shortcoming of the model is the choice of plastic potential, see Equation (5). The Raghava function predicts dilation at all pressure states except for the special case of β = 1, where the plastic deformation is incompressible. On the other hand, experimental evidence shows a contraction effect for PVC in plastic compression, while HDPE behaves close to isochoric, i.e. no change of volume.

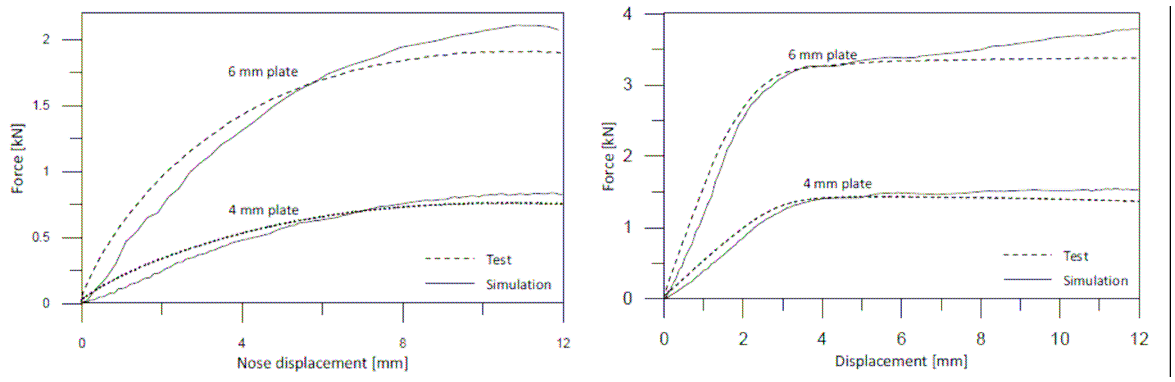

(a) (b)

Figure 7: Force-displacement curves from bending tests with R = 3mm [8]. (a) HDPE. (b) PVC.

Finally, Figure 8 compares the longitudinal normal strains in the tests and simulations, now addressing a 10mm thick specimen with DIC instrumentation. Again, the agreement is acceptable. Figure 8 indicates that the tension strains have a larger absolute value than the compression strains, and a more closely look at the data reveals that 75% of the middle section is in tension.

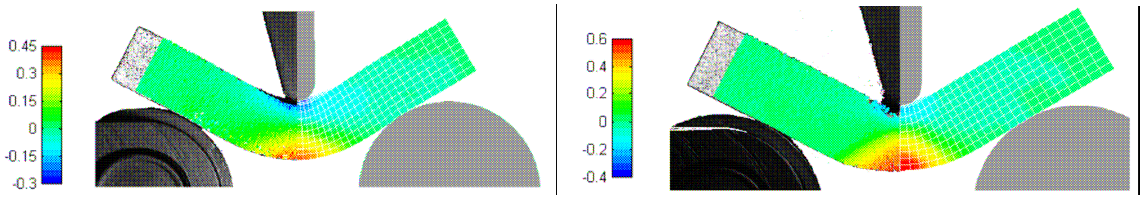

(a) (b)

Figure 8: Strain field from DIC measurements (left-hand part) and simulations (right-hand part) at 10mm deformation. Nose radius R = 3mm and plate thickness 10mm [8]. (a) HDPE. (b) PVC.

6. CONCLUSION AND PERSPECTIVES FOR FURTHER WORK

This paper outlined a new hyperelastic-viscoplastic constitutive model for thermoplastics. The model consists of two fractions sharing the same deformation gradient, and accounting in turn for the intermolecular resistance by pressure-dependent, non-associated hyperelastic-viscoplasticity, and the network resistance by hyperelasticity for compressible rubber-like materials. The constitutive relation is implemented as a user-defined model in LS-DYNA, currently working for brick elements.

The 11 non-zero parameters of the proposed model were determined for two materials, HDPE and PVC, applying data from uniaxial tension and compression tests at different strain rates. The experimental set-up included a digital camera, facilitating the determination of true stress-strain curves. Both materials exhibit significant strain-rate sensitivity. PVC has also a strong pressure-dependent response.

The calibrated model was employed in numerical simulations of a tension test coupon and three-point bending tests. The force-displacement curve and the strain field as found in the experimental test were rather well captured in the simulations.

The choice of the Raghava-like plastic potential is not the optimal one for all materials and loading situations. A closer look at the PVC tension samples reveal a significant voiding process. Also some PP materials experience a significant void growth process during plastic deformation in tension, see Delhaye et al. [9, 10]. An option might be to employ a potential which is function of the damage in the material. Moreover, the relationship between the void growth and macroscopic volumetric strains should have some more attention. Finally. visco-elastic effects are not incorporated in the model presented herein, but they are probably of minor importance for problems involving monotonic loading and large plastic deformations.

REFERENCES

[1] Polanco-Loria M, Clausen AH, Berstad T and Hopperstad OS: Constitutive model for thermo-plastics with structural applications. *International Journal of Impact Engineering* **37** (2010) 1207-1219.

[2] Boyce MC, Socrate C and Llana PG: Constitutive model for the finite deformation stress–strain behavior of poly(ethylene terephthalate) above the glass transition. *Polymer* **41** (2000) 2183-2201.

[3] Haward RN and Thackray G: The use of a mathematical model to describe isothermal stress-strain curves in glassy thermoplastics. *Proceedings of the Royal Society of London Series A (Mathematical and Physical Sciences)* **302** (1968) 453-472.

[4] Raghava R, Caddell RM and Yeh GSY: The macroscopic yield behaviour of polymers. *Journal of Materials Science* **8** (1973) 225-232.

[5] Anand L: A constitutive model for compressible elastomeric solids. *Computational Mechanics* **18** (1996) 339-355.

[6] Livermore Software Technology Corporation: LS-DYNA Keyword User's Manual. Version 971 (2007).

[7] Moura RT, Clausen AH, Fagerholt E, Alves M and Langseth M: Impact on PEHD and PVC plates – Experimental tests and numerical simulations. *International Journal of Impact Engineering* **37** (2010) 580-598.

[8] Hovden MT: Tests and numerical simulations of polymer components. MSc thesis, Dept. of Structural Engineering, NTNU (2010).

[9] Haugen M: Tests and Numerical Simulations of Polymer Components. MSc thesis, Dept. of Structural Engineering, NTNU (2010).

[10] Delhaye V, Clausen AH, Moussy F, Hopperstad OS and Othman R: Mechanical response and microstructure investigation of a mineral and rubber modified poly-propylene. *Polymer Testing* **29** (2010) 793-802.

[11] Delhaye V, Clausen AH, Moussy F, Othman R and Hopperstad OS: Influence of stress state and strain rate on the behaviour of a rubber-particle reinforced polypropylene. *International Journal of Impact Engineering* **38** (2011) 208-218.